All-optical modulation by plasmonic excitation of CdSe quantum dots

DOMENICO PACIFICI[1], HENRI J. LEZEC[1,2] AND HARRY A. ATWATER[1]*

[1]California Institute of Technology, 1200 E. California Boulevard, Pasadena, California 91125, USA
[2]Centre National de la Recherche Scientifique, 3 rue Michel-Ange, 75794 Paris Cedex 16, France
*e-mail: haa@caltech.edu

Published online: 2 July 2007; doi:10.1038/nphoton.2007.95

Photonics is a promising candidate technology for information processing, communication and data storage[1–3]. Essential building blocks, such as logic elements and modulators, have been demonstrated[4–6]. However, because of weak nonlinear light–matter interactions, these components typically require high power densities and large interaction volumes, limiting their application in dense chip-based integration. A solution may be found in surface plasmon polaritons (SPPs), guided electromagnetic waves that propagate with high field confinement along a metal–dielectric interface. We demonstrate an all-optical modulator in which efficient interaction between two light beams at different wavelengths is achieved by converting them into co-propagating SPPs interacting by means of a thin layer of CdSe quantum dots (QDs). The high SPP field confinement and high QD-absorption cross-section enable optical modulation at low power densities ($\sim 10^2$ W cm^{-2}) in micrometre-scale planar devices.

Optical transmission through subwavelength apertures in metal films can be strongly influenced by the presence of nearby surface features, such as grooves or holes[7–9]. Recent studies performed at a specific wavelength (852 nm) have shown that light transmission through a slit milled in an uncoated Ag film can be passively enhanced or suppressed as a result of constructive and destructive interference with an SPP launched by a nearby groove[10,11]. Here we explore the possibility of launching SPPs at various wavelengths (in the range 400–1,500 nm), and demonstrate active control of light transmitted through the slit by optically modulating the amplitude of the SPP. Amplitude modulation of the SPP is enabled by excited-state carrier absorption in CdSe QDs pumped by another SPP at a different wavelength.

A schematic depicting the approach is shown in Fig. 1. We coated with CdSe QDs (ref. 12) a surface-wave interferometer featuring a subwavelength-width slit in a thin metallic film on a transparent substrate, flanked by a single parallel groove etched partially through the metal, with a slit–groove distance D. Two incident beams at different wavelengths ('signal' and 'control' beams, respectively) uniformly illuminate the structure. Diffractive scattering by the groove converts the incident beams into co-propagating SPPs that interact with an active layer of QDs. The total transmitted intensity of the signal beam through the slit is the result of the interference between the incident field (E_0) and the propagating SPP (E_{SPP}) at the slit position; the resulting total transmitted intensity I_T normalized to that of an isolated slit I_0 is given by

$$\frac{I_T}{I_0} = 1 + \eta^2 e^{-\alpha(P)D} + 2\eta e^{-\alpha(P)D/2} \cos[kD(\sin\theta + n_s) + \varphi_g] \quad (1)$$

where $\alpha(P)$ is the absorption coefficient, which we intend to modify with an external control beam of power density P, $k = 2\pi/\lambda$, where λ is the free-space wavelength, n_s is the real part of the effective refractive index of the surface wave, φ_g is an intrinsic phase shift introduced by the groove, θ is the incident angle and η is the overall scattering efficiency of the surface features (see Methods). According to equation (1), a small change in the absorption

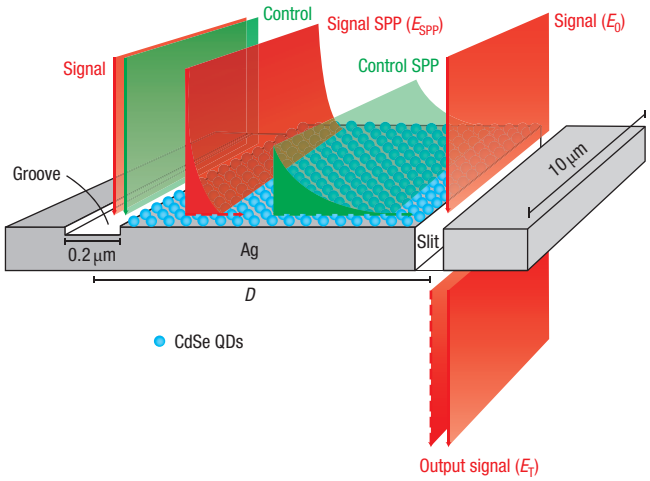

Figure 1 Two-colour all-optical plasmonic modulator. Schematic of a surface wave interferometer consisting of a subwavelength aperture flanked at a distance D by a subwavelength groove milled in Ag, coated with CdSe QDs. A signal and a control beam at different wavelengths uniformly illuminate the device. Diffractive scattering by the groove converts the incident beams into co-propagating SPPs that interact with an active layer of CdSe QDs. The signal beam is transmitted through the slit with an amplitude E_T, which results from the interference between the incident field (E_0) and the propagating SPP (E_{SPP}) at the slit position.

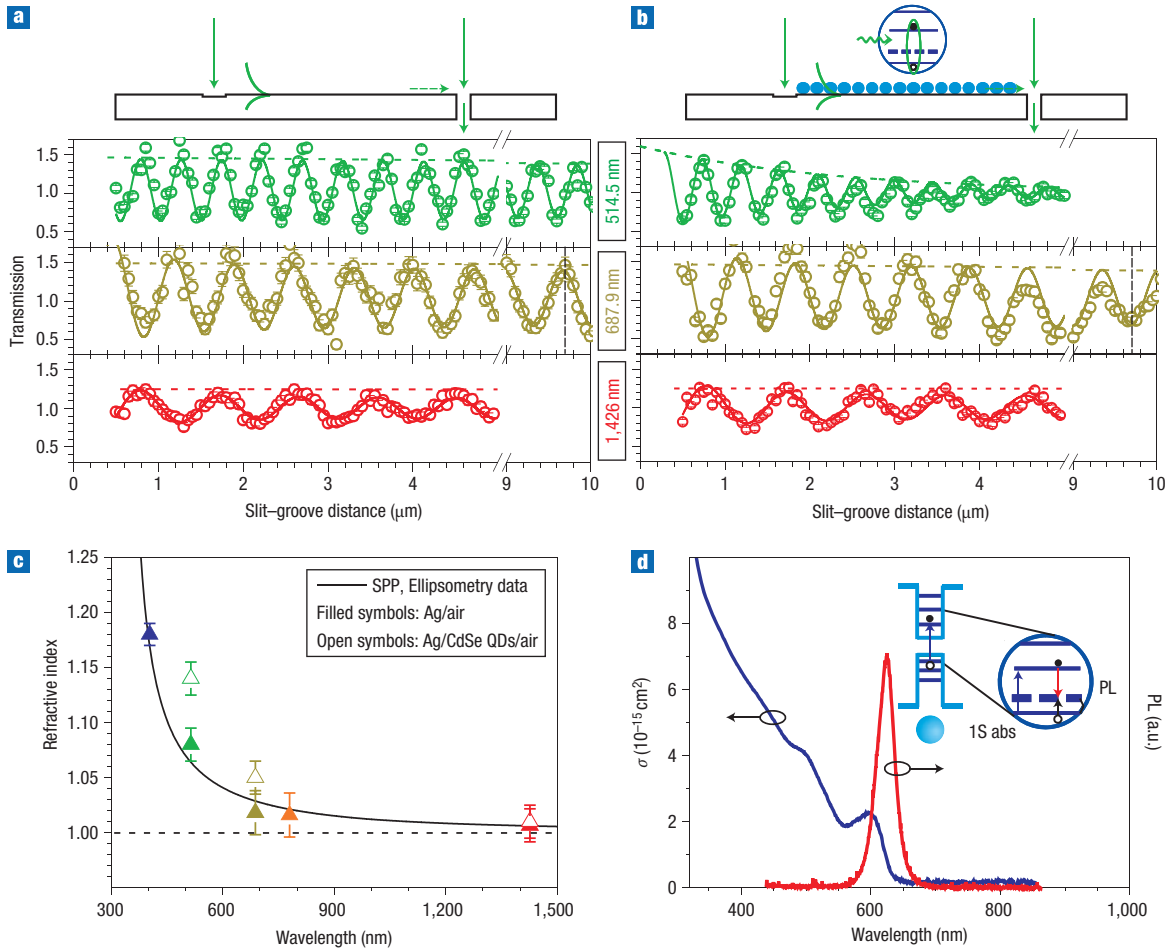

Figure 2 Plasmonic interferometry. **a**, Measurements of the light intensity transmitted through the slit of uncoated interferometers, at various wavelengths. **b**, Transmission for interferometers coated with CdSe QDs. **c**, Surface-wave refractive index for uncoated and QD-coated interferometers. **d**, Absorption σ (blue curve) and photoluminescence (PL) (red curve) spectra for CdSe QDs (indicated by arrows). Inset: energy levels of a QD (refs 15–17). Error bars in **a** and **b** are determined by device-to-device variation in the transmitted intensity and by signal-to-noise ratio; error bars in **c** arise from the fitting procedure of data reported in **a** and **b**.

coefficient $\alpha(P)$ induced by the control SPP will lead to modulation of I_T via attenuation of the signal SPP amplitude.

First we explore the optical properties of an uncoated interferometer. Figure 2a reports measurements of the light intensity transmitted through a set of interferometers milled in an uncoated Ag film (which serve as a reference), at three different laser wavelengths ($\lambda = 514.5$ nm, 687.9 nm and 1,426 nm) as a function of the slit–groove distance D. Data were normalized by the transmitted intensity through an isolated slit milled on the same sample. Several important features are apparent: (1) at a given wavelength λ, the normalized interferometer transmission exhibits an oscillatory behaviour (that is enhanced and suppressed transmission) with increasing slit–groove distance as a result of the constructive and destructive interference between the SPP and the incident beam; (2) the oscillation spatial period increases with increasing λ; (3) the envelope of the oscillation amplitude remains approximately constant as a function of slit–groove distance, suggesting that SPPs can propagate for several micrometres with negligible attenuation. Using equation (1) with k, D and θ as known parameters, fits were performed to the data of Fig. 2a (solid lines), yielding values for η, φ_g, α and n_s at each free-space wavelength λ.

In Fig. 2c, the derived values of n_s are shown as a function of free-space wavelength (filled symbols) and compared (continuous line) with the refractive index for SPPs at a Ag/air interface, $n_{SPP} = \sqrt{\varepsilon_1\varepsilon_2/(\varepsilon_1+\varepsilon_2)}$ (ref. 13) where ε_1 is the real part of the dielectric constant of Ag, experimentally determined by ellipsometry, and $\varepsilon_2 = 1$ is the dielectric constant of air. The excellent agreement clearly confirms in a broad spectral range that the surface wave launched by the groove is indeed an SPP, as theoretically predicted[14].

Next, we explore the effects of a thin layer of densely packed CdSe QDs on the propagation properties of SPPs. In Fig. 2b we show light transmission through surface-wave interferometers coated with CdSe QDs. The addition of the CdSe QD layer causes an increase in the SPP-mode refractive index, as shown by the open symbols in Fig. 2c. For a 9.7-μm-long interferometer (indicated by dashed vertical lines in Fig. 2a and b, $\lambda = 687.9$ nm), a 3% change in refractive index is enough to turn a transmission maximum into a minimum.

The transmission data in Fig. 2b, $\lambda = 514.5$ nm, further reveal that, in the presence of CdSe QDs, the envelope of the intensity oscillations strongly decreases to 1 with slit–groove distance, approaching the value of an isolated slit. This suggests that the thin CdSe QD film strongly attenuates

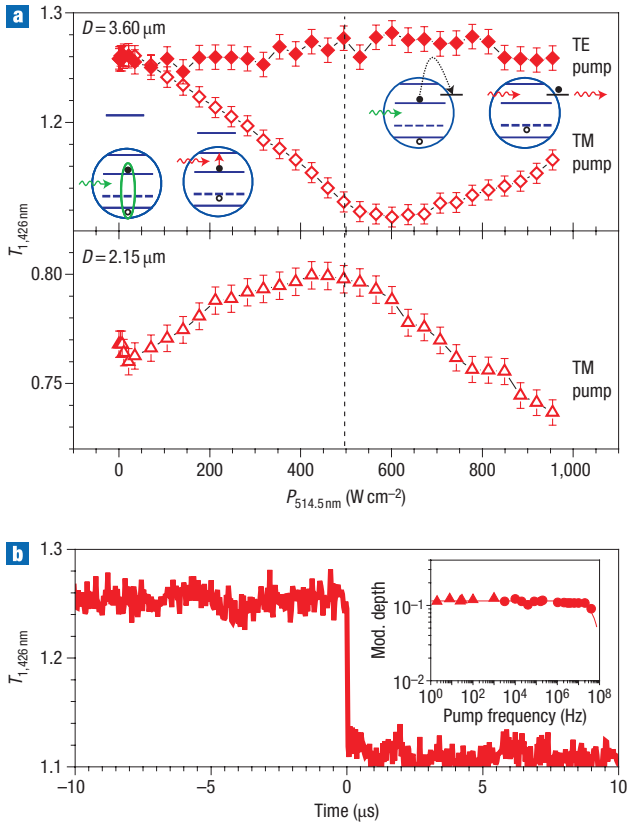

Figure 3 All-optical modulation. a, Open symbols: probe beam transmitted intensity versus pump power density for two QD-coated interferometers. Filled symbols: probe transmission versus power density of a TE-polarized pump beam. Inset schematics: left, attenuation of the probe SPP by an excited QD; right, photobleaching of a QD. Error bars arise from transmitted intensity signal-to-noise ratio. **b**, Variation of the probe intensity transmitted through the slit of a 3.6-μm-long interferometer as a function of time. Inset: variation of the probe signal as a function of pump beam modulation frequency, at a power level of 500 W cm^{-2}.

the SPP launched by the groove, so that at sufficiently long slit–groove distances the SPP is completely absorbed and cannot reach the slit, thus being no longer able to interfere with the incident beam at the slit. Indeed, the absorption coefficient α at $\lambda = 514.5$ nm, as determined from a fit of the data using equation (1), increases from 400 cm^{-1} to 8,200 cm^{-1} upon introduction of the CdSe QD layer. This 20-fold increase in absorption of a propagating SPP results from the high SPP-mode overlap with the CdSe QDs, whose absorption and emission properties are respectively shown as blue and red lines in Fig. 2d, together with a schematic of the energy levels[15–17]. The absorption cross-section of CdSe QDs has been determined by optical measurements of the extinction coefficient of the QDs, as reported in ref. 16. The measured absorption cross-section for CdSe QDs at 514.5 nm is $\sigma \approx 3.5 \times 10^{-15}$ cm^2. Given a nanocrystal density $\rho \approx 10^{19}$ cm^{-3}, and a calculated SPP-mode overlap Γ of ~25%, we estimate an absorption coefficient in the film of $\alpha = \Gamma\sigma\rho \approx 8{,}750$ cm^{-1}, in good agreement with the measured value. Surface plasmon polaritons with energy above the CdSe QD bandgap can be efficiently absorbed in exciton generation in the CdSe quantum dots, and SPPs having an energy smaller than the QD bandgap (such as at $\lambda = 1{,}426$ nm, Fig. 2c) propagate without absorption.

Finally we investigated the transmission of the QD-coated devices under simultaneous illumination with two laser beams at different wavelengths. The possibility of exciting multiple SPPs has been previously explored, for example, by Lereu, Passian and co-workers[18–20]. Experiments were performed in the Kretschmann configuration[21], which makes use of a prism to evanescently couple incident light into SPPs on an uncoated thin film of gold. The authors observe low-frequency modulation of a visible SPP induced by thermal effects on the gold film caused by an infrared SPP.

Here, we instead demonstrate optical carrier excitation as a route to non-thermal modulation of an infrared SPP by means of a visible SPP, launched by a subwavelength object and propagating in a compact waveguide geometry. We performed a two-SPP transmission measurement using a modulated control (pump) SPP ($\lambda = 514.5$ nm) and a continuous signal (probe) SPP ($\lambda = 1{,}426$ nm), as shown in Fig. 1. Interestingly, the transmitted infrared probe intensity for an interferometer with a slit–groove distance $D = 3.6$ μm (which yields a relative maximum in transmission at 1,426 nm) decreases as a function of increasing pump power (Fig. 3a), reaching a minimum at a power density of ~600 W cm^{-2}. A decreased transmission with increasing pump power is consistent with attenuation of the probe SPP due to a pump-activated absorption process. In this process, the pump SPP at $\lambda = 514.5$ nm generates quantum confined electron–hole pairs, at most one per QD. The excited electrons are then able to absorb the probe SPP at $\lambda = 1{,}426$ nm, by undergoing an intraband transition (schematic on the left inset of Fig. 3a). The dynamics of this mechanism have been extensively studied in thick CdSe QD films by femtosecond transient absorption spectroscopy in the visible and near-infrared ranges[22,23].

The experiment is repeated by uniformly illuminating the device with a transverse-electric (TE)-polarized pump beam, for which no long-range SPP can be launched by the groove. The results show no detectable modulation of transverse-magnetic (TM)-polarized probe beam transmission as a function of incident pump power (Fig. 3a, filled symbols). This proves that transmission modulation for TM-polarized pump beams results from pump SPP-induced generation of excitons in CdSe QDs rather than either the direct excitation of the QDs by the incident pump photons or thermal effects due to the incident pump radiation.

Figure 3b illustrates the temporal response of the probe signal to the pump excitation, for a 3.6-μm-long interferometer. At $t = 0$ μs the pump beam, modulated at a frequency of 250 Hz, is turned on at a power density of 500 W cm^{-2}, and the probe transmission intensity shows an abrupt decrease. The switching time of the device is below the temporal resolution of our experimental set up (~40 ns).

In order to better establish the timescale for the modulation effect, the frequency response of the probe signal to pump modulation (inset, Fig. 3b) was measured from 1 to 1,000 Hz using a mechanical chopper, a Ge detector and a lock-in amplifier (triangles), and from 250 Hz to 50 MHz using an acousto–optic modulator, a photomultiplier-tube (PMT) detector extended in the near infrared and a multichannel scaler (circles). The change in probe signal as a function of pump modulation frequency is constant up to 25 MHz, which establishes a timescale of <40 ns for the modulation effect (the roll-off at the end of the explored frequency range corresponding to the response time of our measurement system).

The inferred response time of the device at <40 ns is consistent with our suggested mechanism for device operation, consisting of

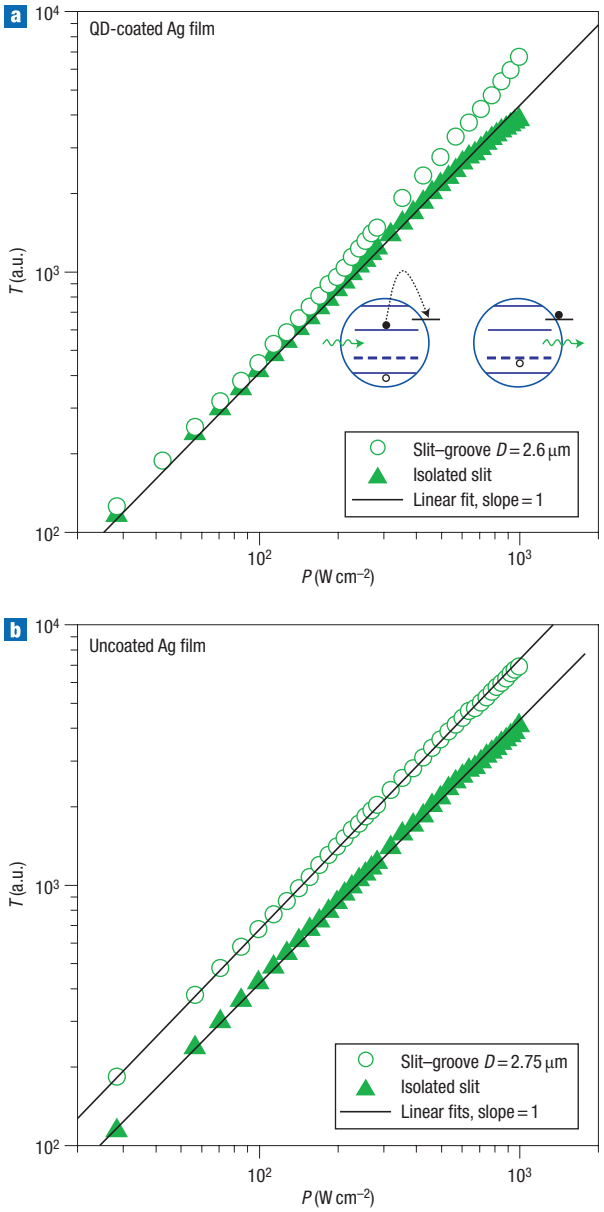

Figure 4 Power dependence of the pump transmission. a, Transmitted intensity at $\lambda = 514.5$ nm as a function of power for a QD-coated surface-wave interferometer with $D = 2.6$ μm (open symbols), and an isolated slit (filled symbols). Inset: schematic diagram of photo-induced bleaching in a QD. **b**, Transmitted intensity at $\lambda = 514.5$ nm as a function of power for an uncoated interferometer.

probe SPP absorption by a fast intraband transition in the CdSe quantum dots excited by the pump SPP. The data reported in Fig. 3b clearly demonstrate the possibility of achieving modulation frequencies that are orders of magnitude faster than typical frequency responses of modulators relying on thermal effects, which can be as low as 40 Hz (ref. 18).

Furthermore, we explored the effects of pump and probe SPPs on an interferometer, which shows a transmission minimum at $\lambda = 1{,}426$ nm in the absence of the pump beam, due to destructive interference. In this case (Fig. 3a, bottom panel), absorption of the probe SPP in the QDs yields a reduced destructive interference with the incident probe beam, and the transmitted intensity is seen to increase, approaching that of an isolated slit.

At power densities >600 W cm^{-2}, both interferometers of Fig. 3a experience a recovery of their original (that is, zero-pump) transmission values, owing to a reduction in absorption of the probe SPP from excited QDs. In Fig. 4a, the transmission intensity at $\lambda = 514.5$ nm for an interferometer with a 2.6-μm slit–groove distance in the presence of CdSe QDs is shown to increase as a nonlinear function of pump power (open symbols). The transmission is at first equal to that of an isolated slit, due to QD-absorption of the SPP. At high pump powers, the transmission reaches values typical for an uncoated device (Fig. 4b, open symbols), in which no absorption from the QD occurs. The decrease in probe-SPP attenuation at high pump excitation rates is due to a two-photon process in which a pump SPP is absorbed by a previously excited QD, producing an electronic photo-ionization event that leads to charge trapping at nearby surface states. The QD is thereafter transparent to either incoming pump or probe SPPs (schematic inset of Fig. 4a). On the other hand, Fig. 4b indicates that pump transmission through an uncoated interferometer is instead linear at all powers, further confirming that the modulation effect observed in the QD-coated sample is not due to thermal effects in the metal film, but to plasmon-induced absorption in the QDs.

We note that a pump power density of approximately 100 W cm^{-2} impinges on a groove area of 2×10^{-8} cm^2, so the total power incident on the groove is 2 μW. The coupling efficiency into an SPP is ~10%, so the pump SPP power is ~200 nW, or ~20 nW μm^{-1} of groove length. Thus, a 1-μm-long groove would enable modulator power operation at 20 nW. All-optical modulation using similarly low incident pump powers has been demonstrated by Soares *et al.*[24] in a different system, in which modulation of a probe optical signal is achieved by a phase transformation in a Ga nanoparticulate, thermally induced by a pump beam. However, owing to the typical dimensions of the nanoparticulate, the power densities needed to operate the device are orders of magnitude higher than in our design. In our scheme, based on intraband electronic transitions in QDs, the modulation switching time is ultimately limited by the QD-exciton recombination lifetime (<40 ns in our system), yielding an estimated minimum switching energy per operation of approximately 800 aJ. These results suggest the potential of our approach for chip-based all-optical modulator arrays whose switching energies may rival those of fully scaled Si-based CMOS electronic inverters[1].

METHODS

THEORETICAL FRAMEWORK

When a TM-polarized plane wave with free space wavelength λ (and free space wavevector $k = 2\pi/\lambda$) impinges on the interferometer at an angle θ with respect to the normal, the subwavelength groove couples a fraction β of the incident field amplitude E_0 into an SPP wave of amplitude E_{SPP} (whose propagation direction is represented with a dashed arrow in Fig. 1). The SPP then propagates along the surface and interferes with the incident light at the slit. The SPP reaches the slit with an overall phase shift:

$$\varphi = kD\sin\theta + k_s D + \varphi_g + i\frac{\alpha}{2}D, \qquad (2)$$

where the first term is the phase shift due to the free-space optical path length difference between the incident wavefronts reaching the aperture and the groove, the second term is the phase shift accrued by the SPP travelling with surface wavevector $k_s = n_s k = n_s 2\pi/\lambda$ (where n_s is the real part of the SPP effective refractive index), and the third term is the phase shift introduced by scattering at the groove. The fourth imaginary term in equation (2) accounts for absorption

or scattering of the SPP (where $\alpha = 4\pi\kappa/\lambda$ is the overall absorption coefficient, and κ is the imaginary part of the SPP effective refractive index).

At the slit entrance, both the directly incident light of amplitude E_0 and the propagating SPP arriving from the groove are partially coupled into guided slit modes through diffractive scattering, with respective amplitude fractions γ and δ. The wave amplitudes contributed by the groove ($E_{T,g}$) and by the slit ($E_{T,s}$) emerging from the slit are respectively given by $E_{T,g} = T\delta\beta e^{i\varphi} E_0$ and $E_{T,s} = T\gamma E_0$, where T is the transmission coefficient of the slit, and $e^{i\varphi}$ accounts for the phase difference between the surface wave and the incident wave at the slit position. The two contributions can interfere if spatial and temporal coherence is maintained between them. The total transmitted amplitude through the aperture is then given by the sum $E_T = T\gamma E_0 + T\delta\beta e^{i\varphi} E_0$. Experimentally we have access to the transmitted intensity:

$$I_T = |E_T|^2 = I_0|1 + \eta e^{i\varphi}|^2 \quad (3)$$

where $I_0 = |T\gamma E_0|^2$ is equivalent to the intensity transmitted through an isolated slit (that is, not flanked by a groove), and $\eta = \delta\beta/\gamma$ regroups the scattering efficiencies of the surface features. Equation (1) in the main text directly follows from equations (3) and (2).

FABRICATION

Surface-wave interferometers consisting of slit–groove pairs with varying slit–groove separation distance D were fabricated by FIB milling (FEI Nova-600 Dual-Beam system, Ga^+ ions, 30 keV) of samples consisting of a 400-nm-thick layer of Ag evaporated onto flat fused silica microscope slides, spin-coated with a 24-nm-thick film of densely packed CdSe QDs. The thickness and uniformity of the QD layer was determined by cross-sectional SEM, AFM and ellipsometer measurements. The CdSe QDs were chemically synthesized in solution (following the method of ref. 12). Multiple spin-coatings of the toluene solution containing CdSe QDs were performed at 1,000 r.p.m. for 1 min, followed by a thermal treatment at 150 °C for 5 min. The groove and the slit were respectively 200 nm and 100 nm wide, 10 μm long, 100 nm and 400 nm deep. The slit–groove distance was systematically varied in the range 500–10,400 nm, in steps of 50 nm, with a positioning accuracy of 1%.

MEASUREMENT SET UP

For the transmission measurements, the laser beam was aligned to the optical axis of a Zeiss Axiovert 135 inverted microscope by using a quartz cube beamsplitter, and focused at normal incidence onto the sample surface (air side) through the microscope condenser. The light intensity transmitted through the aperture of each device was then gathered by a ×50 microscope objective with a numerical aperture of 0.45, sent to a single grating monochromator (Oriel Instrument, Mod. MS257) and detected with a liquid-nitrogen-cooled CCD array detector (100 × 1,340 pixels, Princeton Instruments SPEC-10 System, 400–900 nm wavelength range), with a liquid-nitrogen-cooled ultrasensitive germanium detector (Edinburgh Instruments, Mod. EI-L, 800–1,700 nm wavelength range), or with a photomultiplier tube with an extended near-infrared spectral response (Hamamatsu R5509, range 300–1,700 nm). Probe light at 1,426 nm was delivered to the sample surface using an optical fibre mounted on a three-axis precision translation stage and forming an angle of 32° with respect to the sample normal. The pump laser beam was modulated using a mechanical chopper (1–1,000 Hz) or an acousto–optic modulator (NEOS Mod. 23080-1). The pump-induced intensity change of the probe signal was measured either with a Stanford SR830 lock-in amplifier having the pump modulation frequency as a reference, or with a multichannel scaler (Stanford Research Systems SR430) having the pump modulation frequency as the trigger.

Received 18 September 2006; accepted 11 May 2007; published 2 July 2007.

References

1. ITRS, International Technology Roadmap for Semiconductors, Emerging Research Devices (2005).
2. Sawchuck, A. A. Digital optical computing. *Proc. IEEE* **72,** 758–779 (1984).
3. Huang, A. Architectural considerations involved in the design of an optical digital-computer. *Proc. IEEE* **72,** 780–786 (1984).
4. Jensen, S. M. The non-linear coherent coupler. *IEEE J. Quant. Electron.* **18,** 1580–1583 (1982).
5. Friberg, S. R. *et al.* Ultrafast all-optical switching in a dual-core fiber nonlinear coupler. *Appl. Phys. Lett.* **51,** 1135–1137 (1987).
6. Jewell, J. L. *et al.* 3-pJ, 82-MHz optical logic gates in a room-temperature GaAs-AlGaAs multiple-quantum-well etalon. *Appl. Phys. Lett.* **46,** 918–920 (1985).
7. Garcia-Vidal, F. J., Lezec, H. J., Ebbesen, T. W. & Martin-Moreno, L. Multiple paths to enhance optical transmission through a single subwavelength slit. *Phys. Rev. Lett.* **90,** 213901 (2003).
8. Schouten, H. F. *et al.* Plasmon-assisted two-slit transmission: Young's experiment revisited. *Phys. Rev. Lett.* **94,** 053901 (2005).
9. Lezec, H. J. & Thio, T. Diffracted evanescent wave model for enhanced and suppressed optical transmission through subwavelength hole arrays. *Opt. Express* **12,** 3629–3651 (2004).
10. Gay, G. *et al.* The optical response of nanostructured surfaces and the composite diffracted evanescent wave model. *Nature Phys.* **2,** 262–267 (2006).
11. Gay, G. *et al.* Surface quality and surface waves on subwavelength-structured silver films. *Phys. Rev. E* **75,** 016612 (2007).
12. Murray, C. B., Noms, D. J. & Bawendi, M. G. Synthesis and characterization of nearly monodisperse CdE (E = S, Se, Te) semiconductor nanocrystallites. *J. Am. Chem. Soc.* **115,** 8706–8715 (1993).
13. Raether, H. Surface plasmons on smooth and rough surfaces and on gratings. *Springer Tracts in Mod. Phys.* **111,** 1–133 (1988).
14. Lalanne, P., Hugonin, J. P. & Rodier, J. C. Theory of surface plasmon generation at nanoslit apertures. *Phys. Rev. Lett.* **95,** 263902 (2005).
15. Klimov, V. I. *et al.* Optical gain and stimulated emission in nanocrystal quantum dots. *Science* **290,** 314–317 (2000).
16. Leatherdale, C. A., Woo, W.-K., Mikulec, F. V. & Bawendi, M. G. On the absorption cross section of CdSe nanocrystal quantum dots. *J. Phys. Chem. B* **106,** 7619–7621 (2002).
17. Nirmal, M. *et al.* Observation of the dark exciton in CdSe quantum dots. *Phys. Rev. Lett.* **75,** 3728–3731 (1995).
18. Lereu, A. L., Passian, A., Goudonnet, J. P., Thundat, T. & Ferrell, T. L. Optical modulation processes in thin films based on thermal effects of surface plasmons. *Appl. Phys. Lett.* **86,** 154101 (2005).
19. Passian, A. *et al.* Surface plasmon assisted thermal coupling of multiple photon energies, *Thin Solid Films* **497,** 315–320 (2006).
20. Passian, A. *et al.* Modulation of multiple photon energies by use of surface plasmons. *Opt. Lett.* **30,** 41–43 (2005).
21. Kretschmann, E. Determination of optical constants of metals by excitation of surface plasmons. *Z. Phys.* **241,** 313 (1971).
22. Klimov, V. I., Schwarz, C. J., McBranch, D. W., Leatherdale, C. A. & Bawendi, M. G. Ultrafast dynamics of inter- and intraband transitions in semiconductor nanocrystals: Implications for quantum-dot lasers. *Phys. Rev. B* **60,** R2177–R2180 (1999).
23. Klimov, V. I. Optical nonlinearities and ultrafast carrier dynamics in semiconductor nanocrystals. *J. Phys. Chem. B* **104,** 6112–6123 (2000).
24. Soares, B. F., MacDonald, K. F., Fedotov, V. A. & Zheludev, N. I. Light-induced switching between structural forms with different optical properties in a single gallium nanoparticulate. *Nano Lett.* **5,** 2104–2107 (2005).

Acknowledgements

The authors acknowledge financial support from AFOSR MURI No. FA9550-04-1-0434.
Discussion and technical support from R. J. Walters, L. A. Sweatlock, T. Carmon, S. J. Kim and E. Marcora are also gratefully acknowledged.
Correspondence and requests for materials should be addressed to H.A.A.

Competing financial interests

The authors declare no competing financial interests.